Few-electron artificial molecules formed by laterally coupled quantum rings

T. Chwiej and B. Szafran
Faculty of Physics and Applied Computer Science, AGH University of Science and Technology, al. Mickiewicza 30, 30-059 Kraków, Poland

(Received 12 September 2008; published 8 December 2008)

We study artificial molecular states formed in laterally coupled double semiconductor nanorings by one, two, and three electrons. An interplay of the interring tunneling and the electron-electron interaction is described, as well as its consequences for the magnetization and charging properties of the system. It is shown that both the magnetic dipole moment generated by the double-ring structure and the chemical potential of the system as function of the external magnetic field strongly depend on the number of electrons and the interring barrier thickness. Both the magnetization and chemical potentials exhibit cusps at the magnetic fields inducing ground-state parity and/or spin transformations. The symmetry transformations are discussed for various tunnel coupling strengths, from rings coupled only electrostatically to the limit of coalesced rings. We find that in the ground states for rings of different radii the magnetic field transfers the electron charge from one ring to the other. The calculations are performed with the configuration-interaction method based on an approach of Gaussian functions centered on a rectangular array of points covering the studied structure. Electron-electron correlation is also discussed.

DOI: 10.1103/PhysRevB.78.245306 PACS number(s): 73.21.La, 73.40.Gk

I. INTRODUCTION

In the eighties semiconductor rings of micrometer size were investigated in quest for signatures of the Aharonov-Bohm effect[1] in conductance measurements.[2,3] In the next decade magnetization produced by persistent currents circulating around semiconductor rings was measured.[4] Subsequent technological advances allowed for fabrication of rings with nanometer radii with detectable quantum-size effects. Nowadays, the quantum rings are produced with the etching[5] or surface oxidation techniques,[6] as well as grown by self-assembly.[7] Transport experiments are performed on open quantum rings,[8] while the closed rings are studied in the context of single-electron charging[7] or optical properties.[9–11] Recently, magnetization signal of large ensembles of semiconductor self-assembled nanorings has been detected.[12]

The theoretical literature on quantum rings is very rich. The authors mainly concentrate on the properties of a single isolated quantum ring.[10,11,13–19] At present there is a growing interest in systems of multiple quantum rings including ring arrays.[20,21] Moreover, double rings are produced in both concentric[22–24] and vertical[25] configurations. The tunnel and electrostatic coupling was theoretically studied for both concentric[26–33] and vertically stacked rings.[32] Recently, states of a single electron in a pair of laterally coupled quantum rings were described.[34] The magnetization generated by planar arrays of interacting quantum rings in the absence of the interring tunneling was also discussed.[21] The purpose of the present paper is to describe the system of up to three electrons in an artificial molecule formed by two quantum rings with the account taken for both the tunnel coupling and the electron-electron interaction. We investigate the competition between the tunnel and the electrostatic coupling, the electron-electron correlation, as well as the charging and magnetization properties. The numerical results are provided for the etched InGaAs/GaAs rings[5] with low indium concentration and consequently low potential depth, which favors the interring tunneling.

The evolution of the single-electron ground state with the magnetic field for artificial molecules formed by quantum rings is significantly more complex than for the double quantum dots. In double dots the role of the magnetic field for the eigenstates of the single electron is limited to reduction in the interdot tunnel coupling.[35] In double rings the magnetic field drives the angular momentum transitions of the single electron within each of the rings.[13] When the tunnel coupling is activated, the single-electron ground state becomes localized at the contact between the rings[34] with the localization strength oscillating in function of the magnetic field with a period corresponding to the flux quantum threading a single ring. For identical rings the single-electron ground state corresponds to a binding orbital[34] and possesses an even spatial parity irrespective of the value of the magnetic field. In this paper we show that in double rings containing a few electrons both the spin and spatial symmetry transitions[36] occur in the external magnetic field. We find that the symmetry transformations in the external magnetic field depend strongly on the interring barrier thickness, and they have quite a different character for various numbers of electrons confined within the double-ring structure. Since the transformations influence strongly the charging and magnetic properties, evidence of the tunnel coupling between the rings should be detectable by measurements of chemical potentials and magnetization.

Our discussion covers asymmetric configurations composed of rings of different radii for which we find that the magnetic field induces an oscillatory switching of the ground-state localization from one ring to the other. This effect can be used to transfer the electron between the rings without a need for applying an external electric field to the system.

In this work we use the configuration-interaction approach, which allows for a numerically exact solution of the Schröedinger equation for a few electrons. Application of the configuration-interaction method to the laterally coupled double ring in the external magnetic field is challenging as

compared to both laterally coupled dots and double rings in concentric and vertical configurations. The basis used for the calculation has to keep track of the angular momentum transitions, which occur in each of the rings separately. However, the total angular momentum cannot be used as a quantum number for selection of the basis set since the system does not possess circular symmetry unlike concentric double or vertically stacked rings. For the purpose of the present study we developed quite a powerful technique in which Gaussian functions are used with centers distributed on a regular array. The presented technique is universal and can be applied to few-electron systems in arbitrary smooth confinement potentials.

This paper is organized as follows. In Sec. II we present the model Hamiltonian, the confinement potential, and the configuration-interaction approach based on a mesh of Gaussian functions. A test of the method for two-electron states is presented and the limitations of the approach are explained. The results are given in Sec. III. We start by single-electron states of a single ring and identical double rings. The discussion is then extended to few-electron states and nonidentical rings. The summary and conclusions are given in Sec. IV.

II. THEORY

We consider the following few-electron Hamiltonian

$$\hat{H} = \sum_{i=1}^{N} \hat{h}_i + \sum_{i=1,j>i}^{N} \frac{e^2}{4\pi\varepsilon_0 \varepsilon r_{ij}}, \tag{1}$$

where $\hat{h}_i$ is the single-electron energy operator, and apply the configuration-interaction approach in which $\hat{H}$ operator is diagonalized in a basis of many-electron wave functions with determined values of total spin S and its projection on the z axis S_z. The basis functions are generated with the help of projection operator[37] as the linear combinations of Slater determinants built of eigenfunctions of a single-electron Hamiltonian

$$\hat{h}_i = \frac{[\hat{\mathbf{p}} + e\mathbf{A}(\mathbf{r}_i)]^2}{2m^*} + V_{\text{ext}}(\mathbf{r}_i). \tag{2}$$

We use the vector potential in a symmetric gauge, $\mathbf{A}(\mathbf{r}) = B(-y,x,0)/2$. The single-electron eigenproblem is diagonalized in the basis

$$\phi_i(\mathbf{r}) = \sum_{\alpha=1}^{N} C_\alpha^{(i)} f_\alpha(\mathbf{r}), \tag{3}$$

where the basis function have the form

$$f_\alpha(\mathbf{r}) = \exp\left(-\frac{(\mathbf{r}-\mathbf{R}_\alpha)^2}{2\sigma^2}\right)\exp\left(-\frac{ie}{2\hbar}(\mathbf{B}\times\mathbf{R}_\alpha)\cdot\mathbf{r}\right). \tag{4}$$

In Eq. (4) the probability density associated with each basis function is a Gaussian centered at point $\mathbf{R}_\alpha = (x_\alpha, y_\alpha)$, σ is responsible for the strength of the localization, and the term with the imaginary exponent introduces the magnetic translation, which ensures the gauge invariance of the basis, or in other words the equivalence of all the basis functions irrespective of their localization center. The centers are distributed on a regular mesh of points (see below). The matrix elements of the Coulomb interaction are integrated according to the procedure explained in the Appendix.

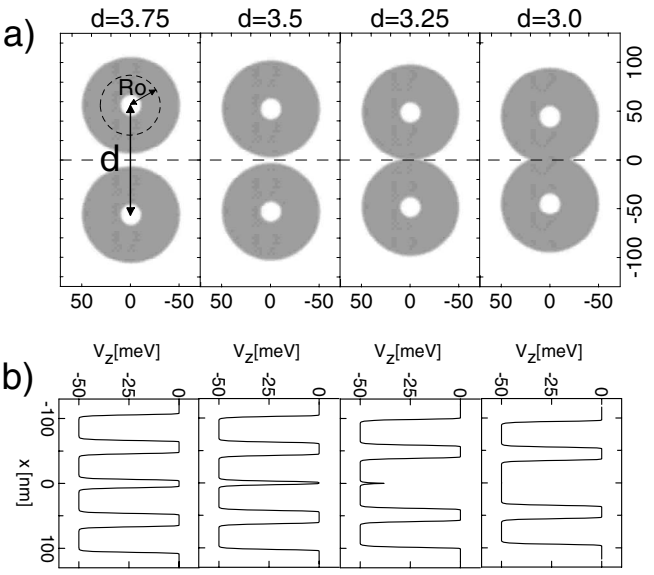

FIG. 1. Double-ring structures for various parameters of the interring distance d and the confinement potential cross sections through the centers of the rings (b) for four values of parameter d.

We model the potential of a single two-dimensional (2D) quantum ring by the formula

$$V_{l(r)}(\mathbf{r}) = -V_0 \exp\left(-\left|\frac{|\mathbf{r}-\mathbf{R}_{l(r)}| - R_0}{\sigma_0}\right|^\alpha\right), \tag{5}$$

where $\mathbf{R}_{l(r)}$ denotes the center of the left (right) ring. We assume $\alpha = 20$ for which the potential is nearly a square quantum well. The other parameters of the rings are adopted for the etched $In_{0.1}Ga_{0.9}As/GaAs$ quantum rings:[5,34] $V_0 = 50$ meV, the radius of single quantum ring $R_0 = 30$ nm, $\sigma_0 = 20$ nm, effective mass of an electron $m^* = 0.05m_0$, and dielectric constant $\varepsilon = 12.4$.

Confinement potential of the double-ring structure is assumed in form

$$V_{\text{ext}}(\mathbf{r}) = \min[V_l(\mathbf{r}), V_r(\mathbf{r})], \tag{6}$$

where $V_l(\mathbf{r}), V_r(\mathbf{r})$ are the confinement potentials of the left and the right quantum ring, respectively. We use a dimensionless parameter d, which describes the distance between the centers of two coupled rings,

$$d = \frac{|\mathbf{R}_l - \mathbf{R}_r|}{R_0}. \tag{7}$$

The confinement potentials of two laterally coupled quantum rings for various d are shown in Fig. 1.

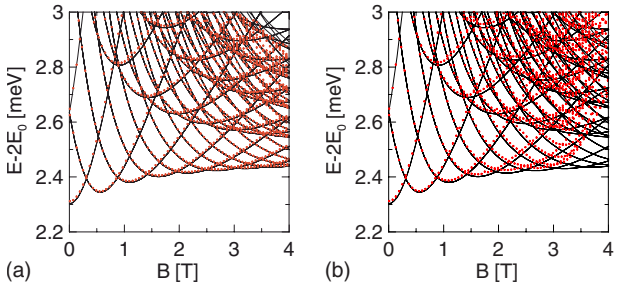

FIG. 2. (Color online) Comparison of the exact two-electron energy spectrum (solid lines) for the 2D harmonic-oscillator confinement potential and the results obtained in the present configuration interaction (CI) method (red dots) for the mesh of 50×50 and 20×20 Gaussians. The energy spectra are calculated with respect to the noninteracting ground-state energy equal to double of the Fock-Darwin (Ref. 36) ground-state energy level.

The centers of the single-electron basis functions [Eq. (4)] are distributed on a mesh of $k_x\times k_y$ points, where $k_x=\frac{(4.8+d)}{4.8}\times k_y$ and $k_y=40$. Moreover, we apply $\sigma=\frac{4.8R_0}{1.4k_y}$. This value was optimized for description of the low-energy part of the single-electron spectrum.

We have tested our method in the problem of two electrons confined in two-dimensional harmonic-oscillator potential, which can be easily solved with the center-of-mass separation technique with an arbitrary precision (the results can be treated as "exact"). We assumed the oscillator energy $\hbar\omega=1$ meV and the calculations were performed in the square region of size $20l_0\times20l_0$, where $l_0=\sqrt{\hbar/m^*\omega}$ is the oscillator length. We have solved the eigenproblem with the configuration-interaction method for basis containing $N=20\times20$ and $N=50\times50$ centers. The exact energy spectra and the results of the present approach are plotted in function of B in Fig. 2.

For the basis with $N=50\times50$ elements, the lower part of the energy spectrum agrees very well with the exact results for magnetic fields up to 4 T. However, for basis with $N=20\times20$ elements, the energy of the ground state is visibly overestimated and the overestimate becomes quite large above 3 T.

For both bases the probability densities are circularly symmetric with respect to the center of the dot for $B=1$ T and $B=3$ T [see Figs. 3(a), 3(b), 3(d), and 3(e)]. For $B=4$ T only the probability density calculated for $N=50\times50$ elements still preserves the confinement potential symmetry. In Fig. 3(g) we plot the mean value of the angular momentum. When the magnetic field increases the ground state becomes more strongly localized and acquires a high angular momentum. For fixed number of centers there is a limitation to the maximal angular momentum that can be described in the single-electron basis. The single-electron states of high angular momenta correspond to sign oscillations of both the real and imaginary part over the angular variable. Clearly, the number of centers in the region where the probability density is nonzero sets the limitation to the maximal frequency of the oscillations. For $B=4$ T the angular momentum obtained in the basis of 20×20 elements is noninteger $\langle L_z\rangle=7.78$ and smaller than the exact ground-state

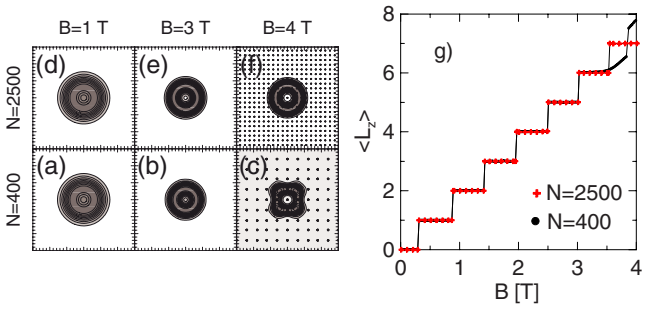

FIG. 3. (Color online) (a)–(f) The total probability densities for $N=50\times50$ and $N=20\times20$ basis centers for two interacting electrons confined in a two-dimensional harmonic-oscillator potential ($\hbar\omega=1$ meV) in the singlet states. The dots in (c) and (f) indicate the centers of Gaussian functions. (g) Expectation values of the total angular momentum for 20×20 elements (points) and 50×50 Gaussian (crosses).

value of $\langle L_z\rangle=7$, which is nevertheless reproduced by the 50×50 basis. Concluding, the present approach allows for a nearly exact solution of the few-electron Schröedinger equation. There is a limitation to the maximal angular momentum that can be accounted for, but the accuracy of the results is easily verified by comparing results of the method produced by various meshes.

III. RESULTS

A. Single-electron single-ring states

The single-electron spectrum for a single quantum ring with potential (6) is shown in Fig. 4. The energy levels plotted with black lines correspond to the lowest state of the radial quantization and the red (gray) ones to the first radial excitation. The energy spacing between these two branches is only about 10 meV, which results of the small depth of the studied structure.

Numbers in Fig. 4 denote the angular momentum. In the ground state the magnetic "period" of the ground-state angular momentum transition is $B_p=1.05$ T, which corresponds

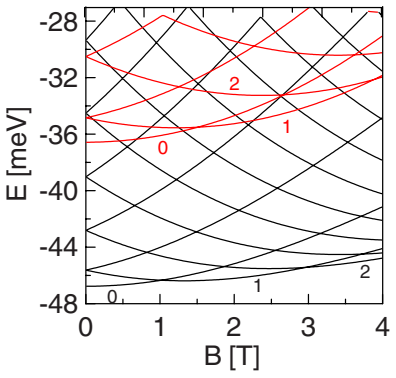

FIG. 4. (Color online) Single-electron spectra for a single quantum ring. Black curves show the energy levels associated with the lowest radial state, and the red (gray) curves the energy levels related to the first radial excitation. Numbers in the figure indicate the angular momentum.

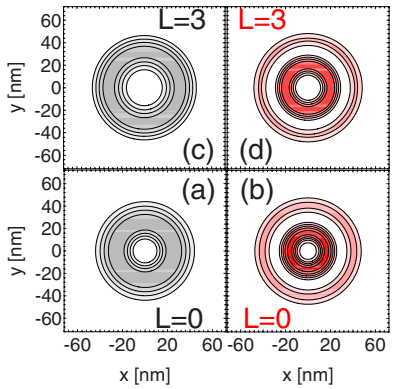

FIG. 5. (Color online) Electron density for the single electron in a single ring in zero magnetic field. Plots (a) and (b) correspond to zero angular momentum and (c) and (d) to $L=3$. Densities in (a) and (c) are obtained for the lowest-energy radial state, and (c) and (d) for the first radial excitation.

to the flux quantum ($B_p \pi R^2 = e/h$) for a strictly one-dimensional (1D) ring of radius $R_{1D}=35.4$ nm, slightly larger than the R_0 parameter (assumed equal to 30 nm) and closer to the average distance from the center of the ring calculated over the radial coordinate of the ring, which is nearly equal to 37 nm. The magnetic period for the first radial excitation is much larger and equals $B_p=1.5$ T, which corresponds to the 1D ring of $R_{1D}=28.9$ nm. The smaller effective radius for the excited radial state than for the ground state may be surprising since usually the excited states occupy larger area than the ground state. In order to explain this feature we plotted the electron densities in Fig. 5 for zero magnetic field. Figure 5(a) shows the density for the ground state and Fig. 5(b) the density for the $L=0$ state of the first radial excitation. Figures 5(c) and 5(d) show the densities of the angular momentum $L=3$ eigenstates—the lowest-energy state and the first-excited state, respectively. We notice that the radial wave functions for $L=0$ are more strongly localized than the ones for $L=3$. This is due to the centrifugal effective potential $\frac{\hbar^2 L^2}{2m\rho^2}$ present in the single-electron Hamiltonian for a single ring written in cylindrical coordinates for the angular momentum L eigenstate

$$H = -\frac{\hbar^2 \partial^2}{2m\,\partial\rho^2} - \frac{\hbar^2 \partial}{2m\rho\,\partial\rho} + \frac{\hbar^2 L^2}{2m\rho^2} + V(\rho) + \frac{m\omega_c^2}{8}\rho^2 - \frac{1}{2}\hbar\omega_c L, \tag{8}$$

where $\rho=\sqrt{x^2+y^2}$. Figure 5 shows that the states that correspond to the radial excitation with electron density forming two concentric rings occupy indeed a larger area than those corresponding to the lowest radial state. However, the inner density ring contains most of the electron charge, and its radius is smaller than the electron-density ring in the lowest-energy radial state [cf. Figs. 5(a) and 5(b), as well as Figs. 5(c) and 5(d)], which explains why the effective radius value R_{1D} obtained for the branch of the excited energy levels is smaller than for the ground state.

B. Single-electron states for a pair of identical rings

The coupling between the rings is of a pure tunnel character for the single-electron states. The single-electron energy spectra are given in Fig. 6 for various interring distances. For $d=3.75$ the tunnel coupling is negligible and the spectrum [see Fig. 6(a)] consists of energy levels which are twofold degenerate with respect to the parity. This energy spectrum is in fact identical with the one of a single separate ring (see Fig. 4). In Fig. 6(b) plotted for $d=3.5$, we spot lifting of the even-odd degeneracy, which occurs when the interring tunnel coupling is activated. Note that when the degeneracy with respect to the parity is lifted, lower energy level always corresponds to the even-parity energy level, i.e., to the binding orbital. The even-odd degeneracy lifted by the tunnel coupling is restored for higher magnetic fields. This results in the attenuation of the tunnel coupling by the magnetic field, which enhances electron localization within each of the rings. For $d=3.25$—when the rings nearly touch one another—the even and odd energy levels differ significantly in the energy. We observe pronounced avoided crossings in the spectrum that occur separately for the even and odd energy levels. The pattern of the avoided crossings in the even and odd parts of the spectrum is similar; only the avoided crossings for the odd energy levels are narrower. The odd-parity energy levels correspond to wave functions vanishing in the center of the tunnel barrier so the tunnel coupling

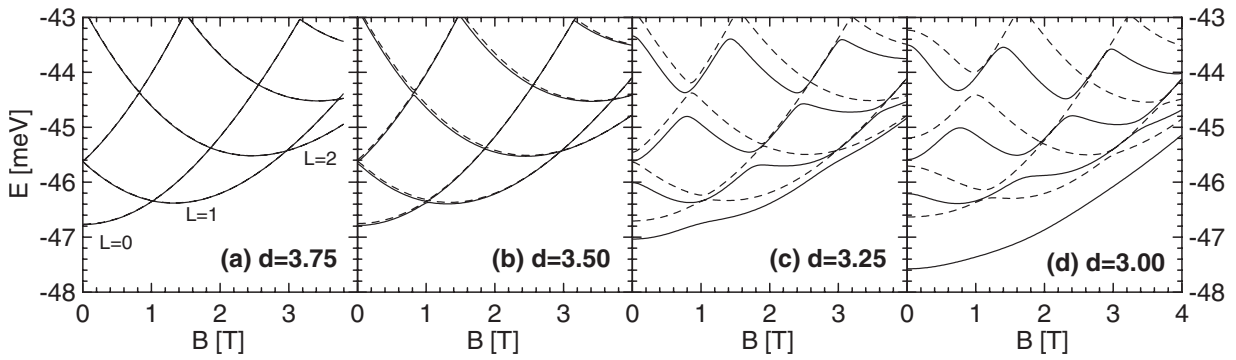

FIG. 6. Single-electron spectra for a pair of identical rings for various interring distances. Solid lines show the even-parity energy levels and the dashed lines the odd-parity energy levels. In (a) the angular momenta with respect to the center of the ring are listed.

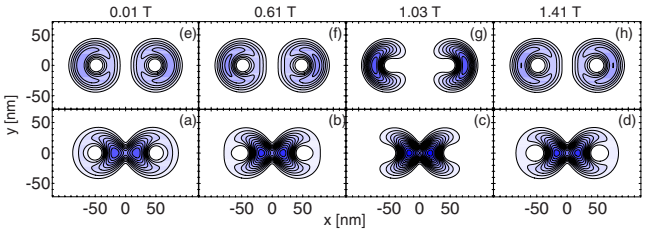

FIG. 7. (Color online) Lower row of plots [(a)–(d)] shows the charge density in the ground state (of the even parity) for $d=3.25$ [the energy levels are given in Fig. 6(c)]. The upper row of plots shows the first-excited state, which is the lowest-energy state of the odd parity. Columns correspond to different magnetic fields.

between the rings is naturally less pronounced than for the even energy levels.

In the absence of the tunnel coupling between the rings ($d \geq 3.75$) the electron density of the stationary states reproduces the circular symmetry of separate rings—irrespective of the magnetic-field value. A distinct dependence on the magnetic field occurs only when the tunnel coupling is present. The charge densities for the lowest even and odd energy levels are given for $d=3.25$ in the lower [(a)–(d)] and upper [(e)–(h)] rows of Fig. 7, respectively. The lowest even (odd) energy level is the ground state (the first-excited state). In the ground state the electron tends to stay near the symmetry center of the double-ring system. The extent of its localization varies with the magnetic field. The strongest localization near the interring contact area [cf. Fig. 7(c)] corresponds to the center of the avoided crossing of the two lowest-energy levels [see the spectrum of Fig. 6(c)]. In the odd-parity energy level the electron is by the symmetry forbidden to be found at the center of the structure and it tends to occupy the extreme ends of rings. The strength of localization at the ends oscillates with the magnetic field and is the largest near the center of the avoided crossings occurring between two lowest odd energy levels [see Fig. 7(g) for $B=1$ T and Fig. 6(c)].

Coalesced rings at $d=3$ form a cavity of increased width near $x=0$ (see Fig. 1), which acts like a quantum dot—in the ground state the electron becomes localized at the interring contact area [Figs. 8(a)–8(c)] and only weakly penetrates the more distant parts of the structure. The ground-state electron density weakly depends on the magnetic field since the electron is localized within an area which is quite small. The energy of this (ground) state is distinctly lowered with respect to the excited part of the spectrum [compare Fig. 6(d) for $d=3$ and Fig. 6(c) for $d=3.25$]. The excited energy levels are essentially unchanged with respect to $d=3.25$; only the avoided crossings become larger. Figure 8 shows that the densities in the first-excited state of the coalesced system are similar to the $d=3.25$ case: they stay spread all over the double-ring structure and are not limited to the contact area as in the ground state. In the spectrum calculated for $d=3.25$ [Fig. 6(c)] a trace of the Aharonov-Bohm oscillation for the ground-state energy is still visible since at least outside the center of the avoided crossings the ground-state wave function encircles the rings (see Fig. 7). For $d=3$ even this residual oscillation of the ground-state energy disappears [see Fig. 6(d)]. However, oscillations are still present in the excited part of the spectrum in which the wave function covers the entire structure. Therefore, the coalescing of the rings mainly perturbs the ground state, which becomes localized in the quantum dot formed at the contact of the rings, and not the excited states, which are spread all over the double-ring structure.

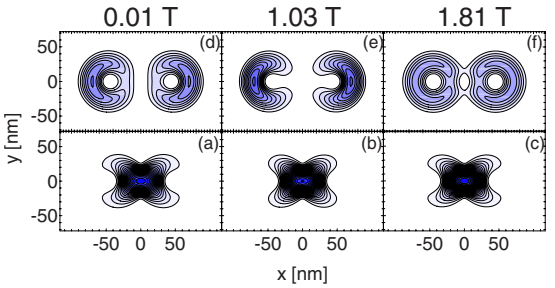

FIG. 8. (Color online) Same as Fig. 7 but for $d=3$. The corresponding spectrum is displayed in Fig. 6(d).

C. Identical rings: two electrons

The electrostatic coupling between the rings appears with the second electron introduced to the system. The two-electron spectrum for a pair of rings is displayed in Fig. 9. For two electrons the Coulomb repulsion makes the interring barrier higher, reducing the tunnel coupling, and in the low-energy part of the spectrum the electrons tend to occupy

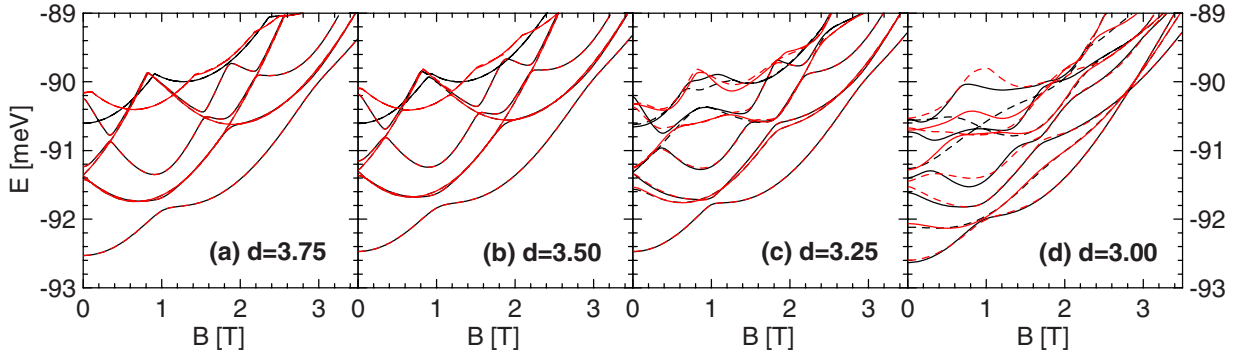

FIG. 9. (Color online) Two-electron spectra for a pair of identical rings. Solid and dashed curves show the even- and odd-parity energy levels. Black and red (gray) lines correspond to the total spin $S=0$ and $S=1$.

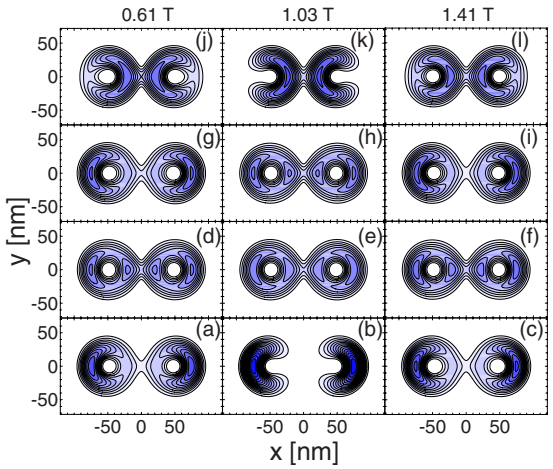

FIG. 10. (Color online) Two-electron densities for $d=3.25$ for four lowest-energy singlet states (for triplets the results are nearly identical). The lower the plot the lower the energy. The ground state [(a)–(c)] and the third-excited state are of the even parity for all B. For $B=1.03$ T the first-excited state is of the even parity and the second-excited state is odd. For the two other magnetic-field values the symmetries of this two energy levels are inverted—see also Fig. 9(c).

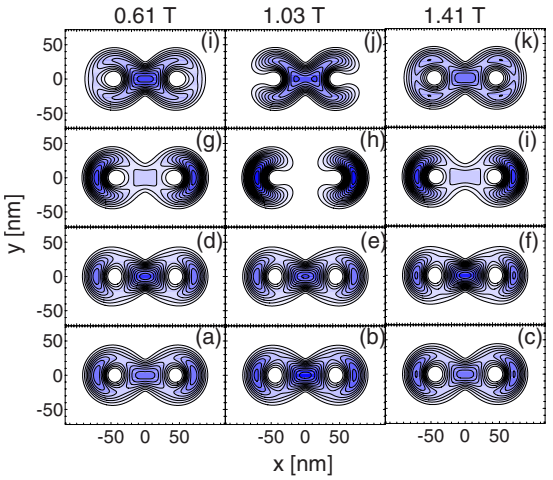

FIG. 11. (Color online) Two-electron densities for $d=3$ for four lowest-energy singlet states. The lower the plot the lower the energy. Plots (a)–(c) correspond to the ground-state.

separate rings. For wide interring barrier and vanishing tunnel coupling the electron separation is complete. In consequence, for $d=3.75$, 3.5, and 3.25 the ground state is twofold degenerate [see Figs. 9(a)–9(c)]. One of the ground states is the spin singlet of the even parity and the other is the spin triplet of the odd parity. In the two-electron systems the singlet-triplet degeneracy (vanishing exchange interaction[38]) occurs when the electrons occupy distinct and separated locations. For double dots this degeneracy is found for wide[38] interring barriers or high magnetic fields. Similar is the effect of the Wigner crystallization in elongated quasi-one-dimensional quantum dots.[39]

For a single-electron the effects of the tunnel coupling—splitting of the odd and even-parity energy levels and avoided crossings in the odd and even parts of the spectrum—were visible already for $d=3.5$ [Fig. 6(b)] and for $d=3.25$ [Fig. 6(c)]; they were quite strong. Lifting of the spin degeneracy is only visible for the coalesced rings [$d=3$, see Fig. 9(d)]. Note that also in this case the singlet and triplet become degenerate for nonzero magnetic field, which enhances the electron localization in opposite ends of the structure.

For wide interring barrier, when the tunnel coupling is absent, the separate rings are only coupled by the Coulomb interaction of confined electrons. The electrostatic potential of the electron localized in one of the rings perturbs the symmetry of the other ring. In consequence the angular momentum of a single ring is not a good quantum number and one obtains avoided crossing between energy levels [Figs. 9(a)–9(c)] instead of the crossings [compare Fig. 6(a)]. Note that the center of the avoided crossing for two electrons [see Fig. 9(a)] occurs for the value of the magnetic field for which the ground-state angular momentum transition occurs for a single electron [cf. Fig. 6(a)].

Electron densities are displayed in Fig. 10 for $d=3.25$. In the ground state the electrons stay at the opposite ends of the rings. The most pronounced separation occurs at the center of the avoided crossing near $B=1.03$ T. Oscillation as pronounced as in the ground state is observed for the third-excited singlet state. In this state the electrons are mostly localized in the center of the structure, in contrary to the ground state, for which the electrons mostly occupy ends of the double structure. The electron density in the third-excited state is in fact similar to the single-electron ground state [cf. Figs. 10(j)–10(l) and Figs. 7(b)–7(d)]. However, the Coulomb repulsion makes the two-electron density less strongly localized. In the first two-excited singlets [Figs. 10(d)–10(i)] the reaction of the density to the field is much weaker than for the ground state and the third-excited singlet.

The singlet electron densities for coalesced rings ($d=3$) are displayed in Fig. 11. Comparison of this plot with the single-electron densities of Fig. 8 indicates that the single-electron ground state [with density localized in the interring contact area—Figs. 11(a)–11(c)] and the first-excited state [electron density localized at the extreme ends of both the rings—Figs. 11(d)–11(f)] contribute nearly equally to the two-electron ground state. In the second [third] -excited state the single-electron first-excited [ground] state contribution is dominant—see Figs. 11(g)–11(i) [Figs. 11(j) and 11(k)]. Note that the type of the electron localization observed here in the second-excited state [Figs. 11(g)–11(i)] corresponds to the two-electron ground state for the larger value of $d=3.25$.

Although in all the low-energy states discussed here for $d\geq 3.5$ the electrons occupy different rings; in fact the type of the interring correlation between the electron positions varies significantly from state to state. Figure 12 shows the pair-correlation function for spin singlet states calculated at $d=3.75$ and $B=0.51$ T for the ground state [Figs. 12(a)–12(c)] and the excited states [Figs. 12(d)–12(l)]. In each of the three columns we assumed that the electron in the left ring is localized in a different position—marked by the dot in Fig. 12. In the ground state the electron in the right ring tends to stay far from the left ring, and the angular

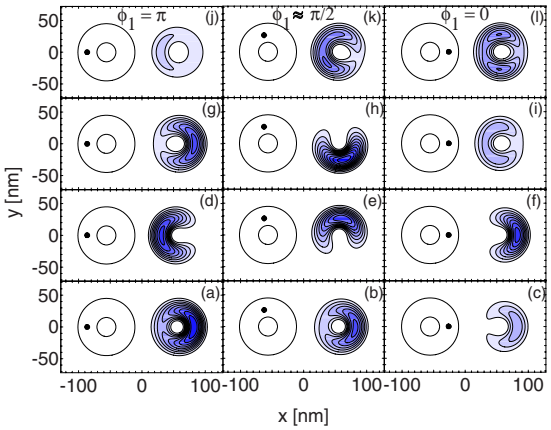

FIG. 12. (Color online) Pair-correlation function plots for spin singlets with the position of the electron in the left ring fixed in the position marked by the dot. The distance parameter is $d=3.75$ and the magnetic field $B=0.51$ T. Lower rows of plots correspond to lower energies.

reaction of the electron in the right ring on the actual position of the electron in the left ring is weak [Figs. 12(a)–12(c)]. Only a slight rotation of the electron probability distribution in the left ring is observed in Fig. 12(b) for the electron in the left ring localized at $\phi=\pi/2$ angle. For the ground state the overall pair correlation function (PCF) values within the right ring are reduced when the electron in the left ring is localized closer to the right ring [see Figs. 12(a)–12(c)—contour scale is kept the same in all the plots]. In the third-excited state an opposite tendency is observed [see Figs. 12(j)–12(l)]: the overall value of the electron probability distribution *increases* when the electron in the left ring approaches the right ring. In this state the minimal PCF value within the right ring is found always near $\phi=0$. In contrast to the ground state and the third-excited state a strong correlation in the angular positions of the electrons is observed for the first- [Figs. 12(d)–12(f)] and second- [Figs. 12(g)–12(i)] excited states.

In the first-excited state the electron in the right ring stays away of the left ring when the electron in the left ring is at $\phi=0$ [Fig. 12(f)], which is natural for repulsing particles. However, when the electron in the left ring is localized above its center $\phi=\pi/2$, the electron in the right ring is also most probable to be found above the center of its ring [Fig. 12(f)] near $\phi=\pi/2$, although one should rather expect a maximum of the probability density at the opposite side of the center. Also in the second-excited state the correlation is somewhat different from what one might expect of the repulsing electrons. For instance when the electron in the left ring is localized at the closest distance to right ring the electron in the left ring tends to approach the left ring [Figs. 12(g)–12(i)].

In order to explain the observed features of the electron-electron correlation in the four lowest-energy singlet states one needs to consider the two-electron wave function. Below we present an approximate analysis for $B\simeq 0.5$ T, when the total wave function is mainly constructed of the single-ring single-electron states of $l=0$ and $l=1$ angular momenta [see Fig. 4], i.e., the single-electron ground state and the first-excited state. Other energy levels lie much higher in the energy. The weak reaction of the electron in the right ring to the angular position of the electron in the left ring observed in the ground state indicates that the two-electron wave function is nearly separable. The spatial part of the singlet ground-state wave function can be written in a following approximate non-normalized form:

$$\Psi = (1+P_{12})\chi_l(r_1)[f_0^l(\phi_1) - cf_1^l(\phi_1)] \times \chi_r(r_2)[f_0^r(\phi_2) + cf_1^r(\phi_2)], \tag{9}$$

where P_{12} is the electron exchange operator,[40] χ_a is the radial wave function of the confinement within the ring a ($a=l$ for the left and r for the right ring), and f_m^a is the angular momentum m eigenstate for the electron localized in the ring a and $f_m(\phi)=\exp(im\phi)/\sqrt{2\pi}$. The argument of f_m^a is the angular coordinate measured with respect to the center of ring a. In Eq. (9) the real-valued $c\geq 0$ introduces mixture of $l=1$ to $l=0$ eigenstates. Mixture of these states is no longer rotationally invariant. For wave function (9) the electron in the left ring is localized preferentially near $\phi=\pi$ and the electron in the right ring near $\phi=0$. For spatially separated χ_l and χ_r radial functions $\chi_l(\mathbf{r})\chi_r(\mathbf{r})=0$ is zero for any $\mathbf{r}$ and the two-electron density is given by

$$|\Psi|^2 = (1+P_{12})|\chi_l(r_1)\chi_r(r_2)|^2|f_0^l(\phi_1) - cf_1^l(\phi_1)|^2 \times |f_0^r(\phi_2) + cf_1^r(\phi_2)|^2. \tag{10}$$

For the first electron fixed within the left ring, $\chi_r(r_1)\to 0$ and P_{12} may be skipped of the above formula since the permutated term vanishes.[40] We are left with the density which is a separable product of single-electron densities whose angular dependence on ϕ_2 becomes independent of ϕ_1, although the overall pair-correlation function value decreases when ϕ_1 approaches 0 (the right ring), in agreement with Figs. 12(a)–12(c).

Now let us turn our attention to the third-excited state. In this state the electrons tend to occupy the area of the contact between the rings, and the PCF shows a weak angular correlation between the electrons [Figs. 12(j)–12(l)] like in the ground state. The wave function which produces these properties differs from Eq. (9) by the sign of c,

$$|\Psi|^2 = (1+P_{12})|\chi_l(r_1)\chi_r(r_2)|^2|f_0^l(\phi_1) + cf_1^l(\phi_1)|^2 \times |f_0^r(\phi_2) - cf_1^r(\phi_2)|^2, \tag{11}$$

for which the electron localization angles are inverted (shifted by π) with respect to the ground state.

In the ground state and in the third-excited state the $l=0$ and $l=1$ single-electron angular eigenstates are mixed *within each of the rings* and the resulting probability densities are (nearly) separable. In the first- and second-excited states the angular momenta $l=0$ and $l=1$ eigenstates contribute in a different manner. In these states the angular momentum of the electron in one of the rings is $l=0$ while the angular momentum of the electron in other ring is $l=1$. This case is described by the following wave function:

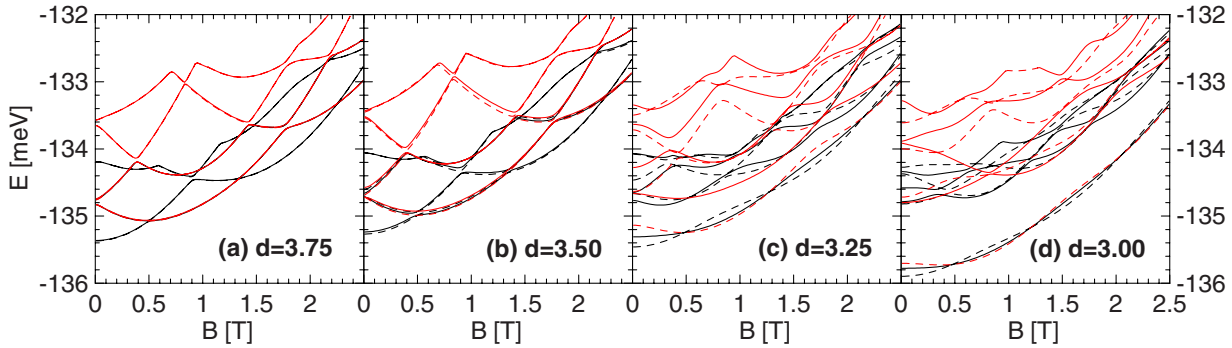

FIG. 13. (Color online) Three-electron spectra for a pair of identical rings. Solid and dashed curves show the even- and odd-parity energy levels. Black and red (gray) lines correspond to the total spin $S=1/2$ and $S=3/2$.

$$\Psi = (1 + P_{12})[\chi_l(r_1)f_0^l(\phi_1)\chi_r(r_2)f_1^r(\phi_2) \pm \chi_l(r_1)f_1^l(\phi_1)\chi_r(r_2)f_0^r(\phi_2)] \quad (12)$$

(for brevity we concentrate on the spin singlets only). At $B=0.51$ T for $d=3.75$ the first (second) -excited singlet is of the odd (even) parity, which corresponds to the "+" ("–") sign in the above formula. In the absence of the overlap between the single-ring wave functions the two-electron density for the first electron fixed in the left ring is given by (up to the normalization constant)

$$|\Psi|^2 \to |\chi_l(r_1)\chi_r(r_2)|^2[1 \pm \cos(\phi_1 - \phi_2)], \quad (13)$$

where ϕ_1 is measured with respect to the center of the left ring and ϕ_2 with respect to the center of the right ring. Formula (13) indicates that in the first-excited state (of the odd parity) both the electrons are most probably localized at the same angle $\phi_1=\phi_2$, and in the second-excited state (of the even parity) the electrons are localized at opposite angles $\phi_1=\phi_2+\pi$, which explains the behavior observed in Figs. 12(g)–12(i). At a close inspection of Fig. 12(h) one notices that the exact angular position ϕ_2 of the maximum in the right ring deviates off ϕ_1 a little bit, which is due to the contribution of the higher angular momenta to the wave functions. We see that in contrast to the ground state and the third-excited state the angular correlations between the electrons are strong in the first- and second-excited states. According to the presented arguments the symmetrization of the wave function by $(1+P_{12})$ operator [as well as the antisymmetrization by $(1-P_{12})$] does not influence the correlated properties of the system when the electrons are spatially separated. Then, (i) the singlet and triplet energy levels become degenerate and (ii) the type of the correlation depends only on the form of the original wave function prior to symmetrization by $(1 \pm P_{12})$. The wave function of the first- and second-excited states that is symmetrized in Eq. (12) is essentially entangled, hence, the strong interring angular correlation. For the ground state and the third-excited state with negligible angular correlations the symmetrization was performed on a strictly separable product of single-electron wave functions.

D. Three electrons in a pair of identical rings

The spectrum for three electrons at wide interring barrier is given in Fig. 13(a). In the ground-state energy level at $d=3.75$ we notice crossings of energy levels related to symmetry transformations which were also present in the single-electron spectrum but which were absent for two electrons. We notice that the "period" of the ground-state energy-level oscillation is halved with respect to the single-ring case [cf. Fig. 6]. In the low-energy spectrum we have two electrons in one ring and a single electron in the other. Halving of the oscillation period results of the fractional Aharonov-Bohm effect[41] occurring for few-electron states confined in a single ring. The ground-state oscillations are due to the spin transformations of the electron pair in a single ring. The angular momentum of the two-electron subsystem is not a good quantum number due to the perturbation of the two-electron ring by the potential of the electron in the right ring. For $B<0.5$ T the ground state is twofold degenerate: with respect to the parity and corresponds to $S=1/2$. For low magnetic fields the spins of the electrons in the single ring are opposite and compensate so the total spin can be identified with the spin of the solitary electron in the other ring. For $B>0.5$ T the ground state of the two-electron subsystem is the spin triplet. Since the spin of the solitary electron may have an arbitrary orientation the ground state becomes fourfold degenerate: with respect to both parity and both the allowed total spin quantum number values $S=1/2$ and $3/2$. For smaller d the degeneracies are lifted [see Figs. 13(b)–13(d)]. Near the ground state we notice a characteristic oscillation of the ground-state symmetry [Figs. 13(c) and 13(d)]. The ground state is mostly either the odd-parity low-spin $S=1/2$ state or the odd-parity spin-polarized state $S=3/2$. When the energy order of these two energy levels changes they become nearly degenerate with a third state: the even-parity low-spin state. The even-parity spin-polarized ($S=3/2$) state runs much higher in the energy. This sequence of the ground-state spin- and parity-symmetry oscillations is also characteristic to three-electron circular[42–44] dots [for circular dots states of angular momentum quantum number which is even (odd) integer are of the even (odd) parity], as well as to elliptic[44] quantum dots and double quantum dots[43] containing three electrons. For elliptic quantum dots the near degeneracy of the three energy levels that we obtain here for discrete values of the magnetic field indicates that the defor-

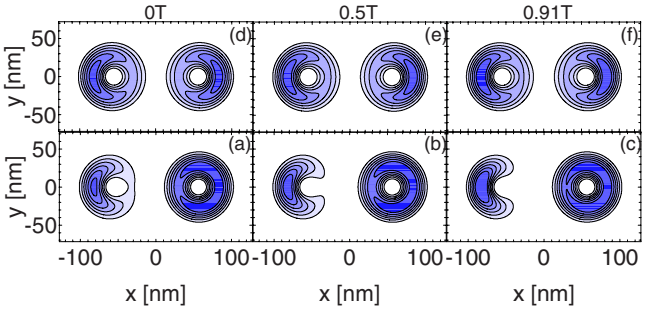

FIG. 14. (Color online) Ground-state charge density for [(d)–(f)] three electrons in identical rings and for [(a)–(c)] the right ring deeper by 0.1 meV at the interring spacing of $d=3.75$.

mation of the confinement potential with respect to the circular limit is strong (see the discussion given in Ref. 44 for elliptic dots). For less strong deformation the even-parity low-spin state becomes a ground state for some narrow but distinct magnetic-field ranges.[43,44]

E. Oscillations of the three-electron charge density with the magnetic field

The results for the charge density of one- and two-electron systems presented above exhibited a distinct magnetic-field dependence. The results for three electrons at $d=3.75$ presented in Figs. 14(d)–14(f) indicate that the dependence on the magnetic field is significantly weaker. For ideally symmetric pair of the rings the charge density of both even- and odd-parity three-electron eigenstates is distributed equally between the rings with 1.5 electron charge per ring on average. A classical distribution with one electron in one ring and two in the other can only occur when the symmetry is lifted. In the absence of the tunnel coupling a potential-well difference of 0.1 meV is enough to obtain the integer distribution of electrons between the rings. The charge density for $d=3.75$ and the right ring deeper by 0.1 meV is shown in Figs. 14(a)–14(c). The dependence of the single-electron charge localized in the left ring on the magnetic field is clear, but the reaction of the two-electron density in the right ring is weaker. Note that in this plot the deviation of the single-electron density off the circular symmetry occurs for $B=0.91$ T, for which the two-electron density is closest to circular, which leads to a compensation of the magnetic oscillation of the density for identical rings.

In order to quantify deviations of the single-ring electron density off the circular symmetry we calculated the parameter

$$D = \langle (x - X)^2 \rangle - \langle (y - Y)^2 \rangle, \tag{14}$$

where X and Y are coordinates of the ring and the average is calculated over the charge density of separate rings. The result is displayed in Fig. 16 with the blue (gray) curve for the two-electron density of the deeper ring and with the black curve for the single-electron density of the shallower ring. The single-electron parameter is larger, varies more strongly with the magnetic field, and its variation is continuous in contrast to the two-electron value, which has cusps when the

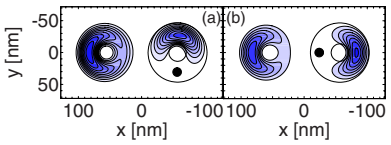

FIG. 15. (Color online) Pair-correlation function for the ground state at $B=0$ and $d=3.75$ for the right ring deeper by 0.1 meV than the left one. Left ring contains a single electron and the right one two electrons. A position of one of the electrons in the right ring is fixed and marked by the dot. Contours of the ring area are also shown.

ground-state spin state of the two-electron subsystem changes. Moreover, the single-electron parameter is positive, which indicates that the deformation occurs rather in the horizontal (x) direction, while the two-electron deviation occurs mainly in the vertical direction (y). The absolute value of the deviation of the two-electron density from circular is the largest at the symmetry transformations. As noted in context of Fig. 14 the largest deformation of the single-electron density corresponds to a weak deformation of the two-electron density.

When the two-electron subsystem changes its spin state the ground-state charge density in the deeper ring is modified in a discontinuous manner. Due to the Coulomb coupling this change may influence the electron density of the shallower ring, which might react in a discontinuous manner. In order to quantify this reaction we calculated derivatives of the D parameter with respect to the magnetic field. The derivative of the two-electron parameter is discontinuous at the cusps [see Fig. 16(b)]. We notice that the single-electron parameter exhibits an irregular structure when the two-electron density changes. However, this structure is not very pronounced. This result, along with the presented above reference calculations, indicates that the charge density of each ring is quite indifferent to the actual form of the charge distribution in the other ring. Additional argument for that conclusion is provided by the pair-correlation function.

The pair-correlation function plot for three-electron system with two electrons in the right ring is shown in Fig. 15 for the ground state at zero magnetic field. We fix a position

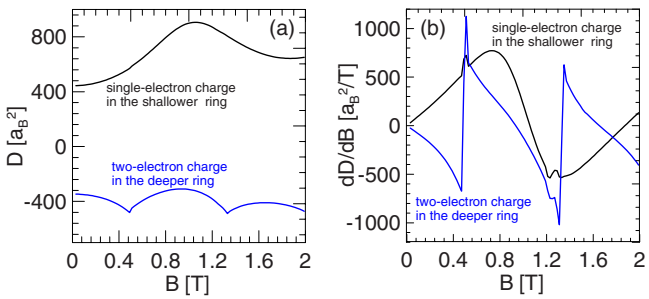

FIG. 16. (Color online) (a) Deviations o the single-ring electron densities off the circular symmetry [Eq. (14)] in function of the magnetic field for the system of three electrons in double-ring structure with the right ring deeper by 0.1 meV for $d=3.75$. Blue (gray) curve corresponds to the deeper ring occupied by two electrons and the black curve to the shallower ring, which contains a single electron. (b) Derivative of D over B. a_B is the Bohr radius.

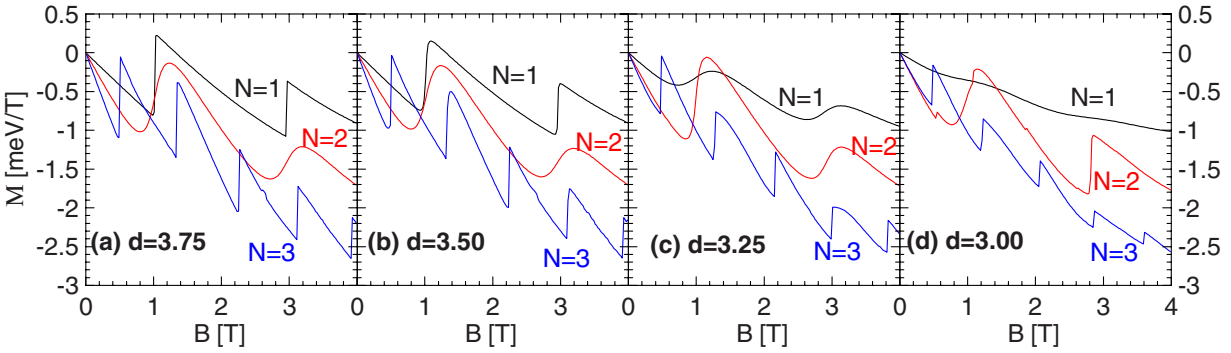

FIG. 17. (Color online) Magnetization of a pair of identical rings filled with one, two, or three electrons plotted with black, red (light gray), and blue (dark gray) curves, respectively.

of one of the electrons in the right ring and mark it with the dot in the figure. We notice that the angular distribution of the solitary electron in the left ring is unaffected by the position of the fixed electron. Only the electron in the same (right) ring reacts to the variation in the fixed electron position [compare Figs. 15(a) and 15(b)]. Note that for the electron fixed below the center of the right ring [Fig. 16(a)], the other electron in the right ring is not exactly on the other side of the center. It tends to avoid the left part of the ring and the position of the maximum is localized below the angle $\phi = \pi/2$. The result of Fig. 15 indicates that in rings separated by a barrier that is thick enough to prevent the interring tunneling, the electrons are mainly coupled as entire charge densities and do not react on their actual position. A strong angular correlation is only observed for the electron within the same ring.

F. Magnetization

Figure 17 shows the magnetization $M = -\frac{\partial E}{\partial B}$ of the pair of identical rings filled by one, two, and three electrons with different spacing parameters d. For a single circular ring the magnetization is discontinuous at the angular momentum transitions. The interring tunnel coupling makes the single-electron magnetization smooth and continuous [see black curves in Figs. 17(a)–17(d)]. The oscillation of M with B are extinguished for the coalesced rings, when the Aharonov-Bohm oscillations occurs only in excited states and not in the ground state, which is localized in the quantum dot formed at the contact of the rings.

For two electrons the magnetization is a smooth function of the magnetic field unless the rings are close enough to form a single structure. Two-electron ground-state symmetry transformations which produce the cusps in the magnetization occur only for the coalesced rings ($d=3$). For three electrons the symmetry transformations are present for any d. For large interring distance they correspond to the spin transformations of the subsystem of two electrons confined within the same ring. The spin transformations of the three electron system occur also when the rings form a single coalesced structure.

We notice that for two separated rings [Fig. 17(a)] the magnetization of the single-electron and two-electron states exhibits the same "periodicity." In both cases the dipole moment oscillation has the magnetic period corresponding to the flux quantum passing through a single ring. The variation in the dipole moment is abrupt for $N=1$ due to the angular momentum transitions and for $N=2$; the dipole moment becomes a continuous function of the magnetic field, which results in mixing of the angular momentum eigenstates by the electron-electron interaction. For $N=3$ one finds two electrons in the same ring. The discontinuous variation in the dipole moment as function of the magnetic field observed in [Fig. 17(a)] is due to the spin transitions of the two-electron subsystem occupying the same ring. Period of the oscillations for $N=3$ is halved with respect to $N=2$ and to $N=1$ states, which is a signature of the fractional Aharonov-Bohm

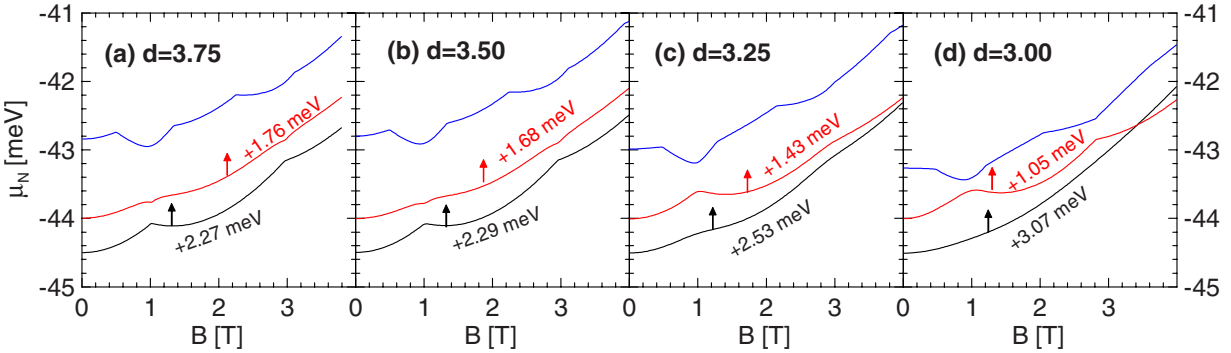

FIG. 18. (Color online) Chemical potential of one, two, and three electrons confined in the double ring plotted with black, red (light gray), and blue (dark gray) curves, respectively.

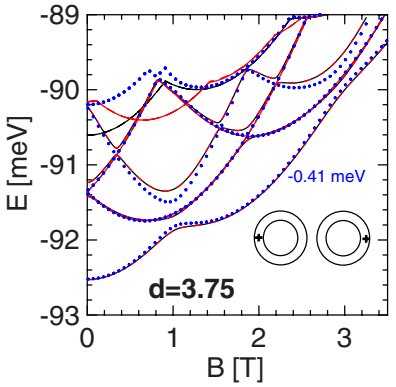

FIG. 19. (Color online) The exact two-electron spectrum (lines) and the reference spectrum (dots) obtained as a sum of single-electron spectra for a single ring perturbed by a classical charge within the other ring. The reference spectrum was shifted down by 0.41 meV on the energy scale. The crosses in the inset show the assumed positions of the classical charges.

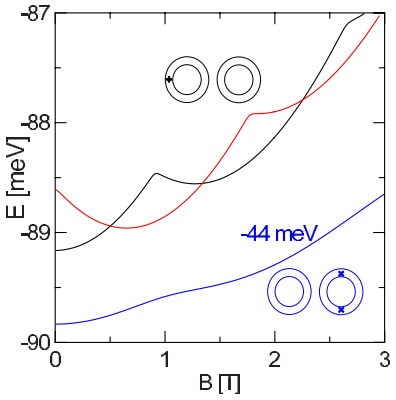

FIG. 20. (Color online) Blue (dark gray) line shows the energy of the single electron (shifted down by −44 meV) within the left ring with the Coulomb potential of two classical point charges localized as indicated in the blue (dark gray) inset to the figure. Black and red (light gray) curves show the lowest-energy singlet and triplet for two electrons in the right ring with a classical point charge localized in the left ring in the position marked in the black inset. Distance parameter between the rings is $d=3.75$ and the depth of the right ring is increased by 0.1 meV.

oscillations.[41] For $N=2$ and $N=3$ the electron distribution between the rings remains essentially unchanged when the interring barrier is reduced, and therefore, the periodicity of the dipole moment does not significantly change with d [Figs. 17(a)–17(d)]. For $N=1$ the oscillations disappear for smaller d [Fig. 17(d)] when the electron occupies the quantum dot formed at the contact between the rings.

G. Charging properties

For a structure embedded in a charge tunable device the charging of the double ring by Nth electron occurs when the chemical potential $\mu_N=E_N-E_{N-1}$ (where E_N is the ground-state energy of N confined electrons) is aligned with the Fermi level of the electron reservoir. In capacitance spectroscopy[7] the cusps of the charging lines in function of the magnetic field indicate symmetry transformations of the confined system.

Figure 18 shows the calculated chemical potentials in function of the magnetic field. Chemical potentials of one and two electrons were shifted up on the energy scale for clarity (the amount of the shift is given in the figure). In the absence of the tunnel coupling [Figs. 18(a) and 18(b)] the chemical potential of two electrons is a smooth function of the magnetic field with exception to the V-shaped cusps that result of the single-electron angular momentum transitions that produce the Λ-shaped cusps on the single-electron chemical potential. Since the two-electron ground-state energy is smooth as a function of B, all the cusps of the three-electron system have the Λ shape and result of the symmetry transformations of the three-electron system. The parabolic minimum of μ_3 between the Λ cusps is due to the smooth maximum of E_2 that occurs at the avoided crossings near odd multiples of flux quanta (see Fig. 9). Due to the fractional Aharonov-Bohm oscillation of the two-electron subsystem we find two Λ cusps in μ_3 for a single one in μ_1.

For $d=3.25$ the Λ cusps of the single-electron chemical potential are smoothed out and in consequence the V cusps of μ_2 disappear [Fig. 18(c)]. The ground-state avoided crossing for the two electrons becomes narrower so μ_2 acquires a distinct maximum near 1 T. A Λ cusp in μ_2 and consequently a V cusp in μ_3 occur for the coalesced rings [Fig. 18(d)]. The presented results indicate that the strength of the interring coupling may be deduced of the charging experiments.

H. Separability of the system at large interring barrier

In the absence of the tunnel coupling the rings are coupled only electrostatically. In order to answer the question to which extent the distinct rings may be treated as separable, we performed reference calculations in which we considered a *single* ring perturbed by the Coulomb potential of a classical point charge localized in the other ring. In the reference calculation for the two-electron system we assumed that in the left (right) ring a classical point-charge electron is localized at $\phi=\pi$ ($\phi=0$) and calculated the single-electron spectrum for the confinement potential of the right (left) ring. The two-electron spectrum of a ring couple was then estimated by the sum of single-electron spectra of the left and right rings.

Comparison of the obtained result with the exact two-electron spectrum is given in Fig. 19. The reference calculation was shifted down by 0.41 meV to coincide with the exact two-electron energy for $B=0$. We see that the magnetic-field dependence of the ground-state energy and the nearly degenerate first-excited energy level is quite accurately described by the ansatz model. In fact the exact first-excited energy level is not exactly degenerate and there are two energy levels for states of different parities. The reference calculation in which the rings are treated separately overlooks this splitting. Although the width of the exact avoided crossing near $B=1$ T is quite accurately described by the reference calculation, the increase in the exact ground-state energy in the center of the avoided crossing is smaller than in the reference calculation. The higher part of the exact

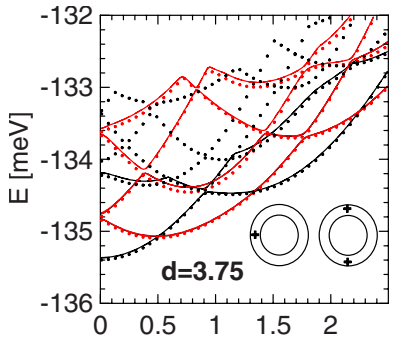

FIG. 21. (Color online) The exact three-electron spectrum (lines) and the reference calculation (dots). The reference spectrum is a sum of a single-electron spectrum in the left ring perturbed by two classical charges and the two-electron spectrum of the right ring with a classical charge localized in the left ring (see the inset to this figure and to Fig. 20). Black color corresponds to the low-spin states and red (light gray) color to the high-spin states. The reference spectrum was shifted down by 1.41 meV.

spectrum deviates off the reference calculation significantly.

The reference spectrum for three electrons was calculated as a sum of two spectra: (1) the single-electron confined within the left ring, which is perturbed by two classical charges localized in the right ring at positions marked by the crosses in the blue (dark gray) inset to Fig. 20 and (2) the two-electron spectrum of the right ring with the classical point charge localized in the left ring in the position of the cross in the black inset to Fig. 20. Blue (dark gray) curve in Fig. 20 shows the single-electron ground state; black and red (light gray) curves correspond to the lowest-energy singlet and triplet states of the two-electron ring, respectively. For a single circular ring the confined electron system undergoes

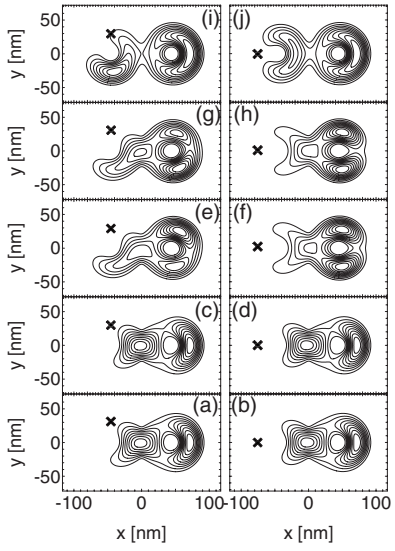

FIG. 22. Pair-correlation function for three electrons in coalesced double-ring structure $d=3$ at $B=0$. Plots (a) and (b) correspond to the ground state and higher rows to subsequent *low-spin* ($S=1/2$) energy levels. The two columns correspond to two locations of the fixed position electron, which is marked by the cross in the figure.

momentum transitions as function of the magnetic field. For the two electrons the transitions are accompanied by the spin transformations. When the two rings—one containing a single electron and the other two electrons—become electrostatically coupled the angular momentum transformations disappear. However, the spin ground-state transitions are still present in the two-electron subsystem.

The reference spectrum for the three-electron system calculated using the two separate calculations is compared to the exact spectrum in Fig. 21. In the ground state both calculations agree quite accurately, but differences are observed in the excited states.

I. Electron-electron correlation in the coalesced double rings

The pair-correlation plots for the three-electron system presented so far were limited to large interring barrier. Let us look at the correlation when the rings form a single structure. The pair-correlation function plots for $d=3$ and $B=0$ are given in Fig. 22 for the low-spin states. Near the ground state one of the electrons occupies the contact area between the rings and the two others are localized at the left and right ends of the double structure. In the plots we present results for two different locations of the electron in the left ring (marked by crosses in Fig. 22). The pair correlation for the lowest-energy odd-parity state Figs. 22(a) and 22(b) and the first-excited state Figs. 22(c) and 22(d) are similar. Both these states have similar energies [see the spectrum in Fig. 13(d)]. Only the electron localized at the contact between the rings reacts to the position of the electron in the left ring, and this reaction is not very pronounced [see Figs. 22(a)–22(d)]. A stronger reaction is observed in the three next-excited states [Figs. 22(e)–22(j)], which correspond to distinctly higher energies [Fig. 13(d)]. In the highest energy state of the presented set the "quantum dot" formed at the contact is empty, and the correlation properties [Figs. 22(i) and 22(j)] are similar to the ground state at large interring barrier [cf. Fig. 15].

Results presented above for wide interring barrier indicated that in the ground state the actual electron positions are correlated only within the same ring. Figure 22 demonstrates that for rings forming a single structure the electron-electron correlation in the ground state still has only a short-range character. In the studied case each of the three electrons occupies a different spatial location and is quite indifferent to the actual positions of the other electrons within their charge islands.

J. Rings of different radii

Results presented so far were obtained under assumption that both the rings have the same size. Let us now consider two rings that possess slightly different radii. Namely, we assume that the radius of the right ring is increased by 5%. The calculated single-electron spectra are displayed in Fig. 23.

The energy of the lowest zero angular momentum state in a single ring increases with its increasing radius (see Fig. 24). For that reason in the absence of the magnetic field the zero angular momentum ground state is localized in the

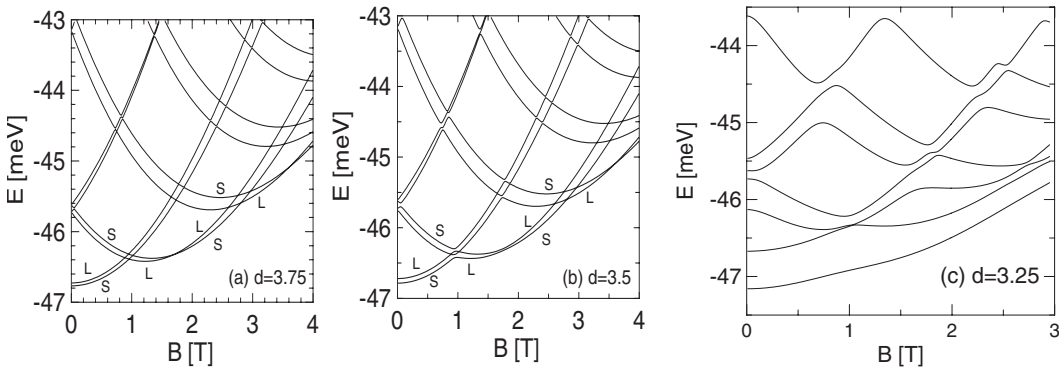

FIG. 23. Single-electron spectrum for a pair of rings of identical depth but with the radius of the right ring increased by 5%. In (a) and (b) states localized mostly within the smaller (larger) ring are labeled by S (l). In (c) electron in the ground state is nearly equally distributed between the rings.

smaller ring [energy levels marked by S in Figs. 23(a) and 23(b)], and the first-excited state is localized in the larger ring (energy levels marked by L in Fig. 23). On the contrary, due to the centrifugal potential at zero magnetic field the states of the nonzero angular momentum have lower energy when localized in the larger ring [see Fig. 23(a)]. When the magnetic field is switched on the energy levels that originate from the positive angular momenta single-ring states go down in the energy due to the interaction of their paramagnetic dipole moments with the external field [see the last term in the Hamiltonian (8)], and they replace the zero angular momentum low-field ground state when B is high enough. Consequently, for B exceeding 1 T the ground state becomes localized in the larger ring. For $B>1.2$ T the ground state (in the larger ring) and the first-excited state (localized in the smaller ring) start to increase in the energy. This increase results in the diamagnetic shift [related to the second term at right of Eq. (8)]. It is a general rule that the diamagnetic shift is stronger for more delocalized states (covering areas of larger ρ). In consequence one obtains another change in the electron localization: above $B=1.8$ T the ground state is localized again in the smaller ring. The ground-state transition to the larger ring occurs again when the states originating from higher angular momenta become ground states. For $d=3.75$ the change in the ground-state localization occurs through crossing of energy levels [see Fig. 23(a)]. Already for $d=3.5$ tunnel-related avoided crossings are obtained [see Fig. 23(b)]. For the strong-coupling case of $d=3.25$ the spectrum resembles the one of the identical rings [cf. Fig. 6(c)].

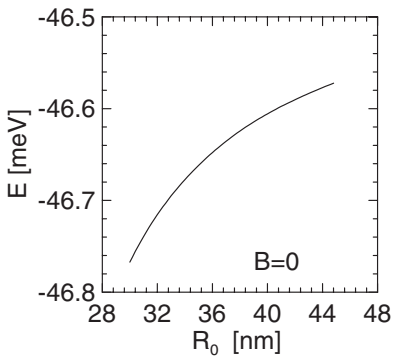

FIG. 24. Ground-state energy in function of the ring radius for a single electron within a single ring.

The shifts of the electron density with the magnetic field between the rings are illustrated in Fig. 25 for $d=3.5$. For low magnetic field the electron in both the ground state and the first-excited state is present in both the rings [Fig. 25(a) for $B=0.5$]. At $B=1$ T we observe an avoided crossing which results in the change in the order of the energy levels corresponding to different single-ring angular momenta. For $B<1$ T ($B>1$ T) the electron in the ground state occupies preferentially the smaller (larger) ring [see Figs. 25(a) and 25(b)]. As the magnetic field increases above 1.25 T the ground-state presence of the electron in the left (smaller) ring is enhanced. Equal electron distribution is obtained near the center of the avoided crossing for $B\simeq 1.75$ T [Fig. 25(c)], and for $B=2.51$ T the ground state is totally localized in the smaller ring. Near $B=2.8$ T in [Fig. 23(b)] we see a change in the order of the energy levels in the ground state. This is a very narrow avoided crossing (which in the figure scale appears as a level crossing). After this avoided crossing the electron in the ground state is localized in the larger ring again. Equal distribution of the ground-state electron between the two rings is found near 3.61 T. The change in the order of the two energy levels in the ground state that occurs here is also accompanied by a narrow avoided crossing. For the magnetic field increased additionally by only 0.2 T the interring tunnel coupling is broken and the ground state and the first-excited state occupy a single ring. We see that at higher magnetic fields—which favor a stronger localization of the confined states—the avoided crossing related to electron transfer between the rings becomes narrower both on the magnetic field and energy scales [compare Figs. 25(a)–25(c) and Figs. 25(d)–25(f)].

To summarize the shifts of the charge in the single-electron problem of a single ring in Fig. 26, we plotted the ground-state charge localized in the left ring for various distance parameters. For $d=3.75$ the charge in the left ring has a steplike dependence on B and is either very close to 1 or very close to zero. The oscillation of the charge for $d=3.5$ becomes less abrupt. For the strong coupling case $d=3.25$ the charge localized in the left ring oscillates around $0.5e$. In all the cases the oscillations of the charge localized in the left

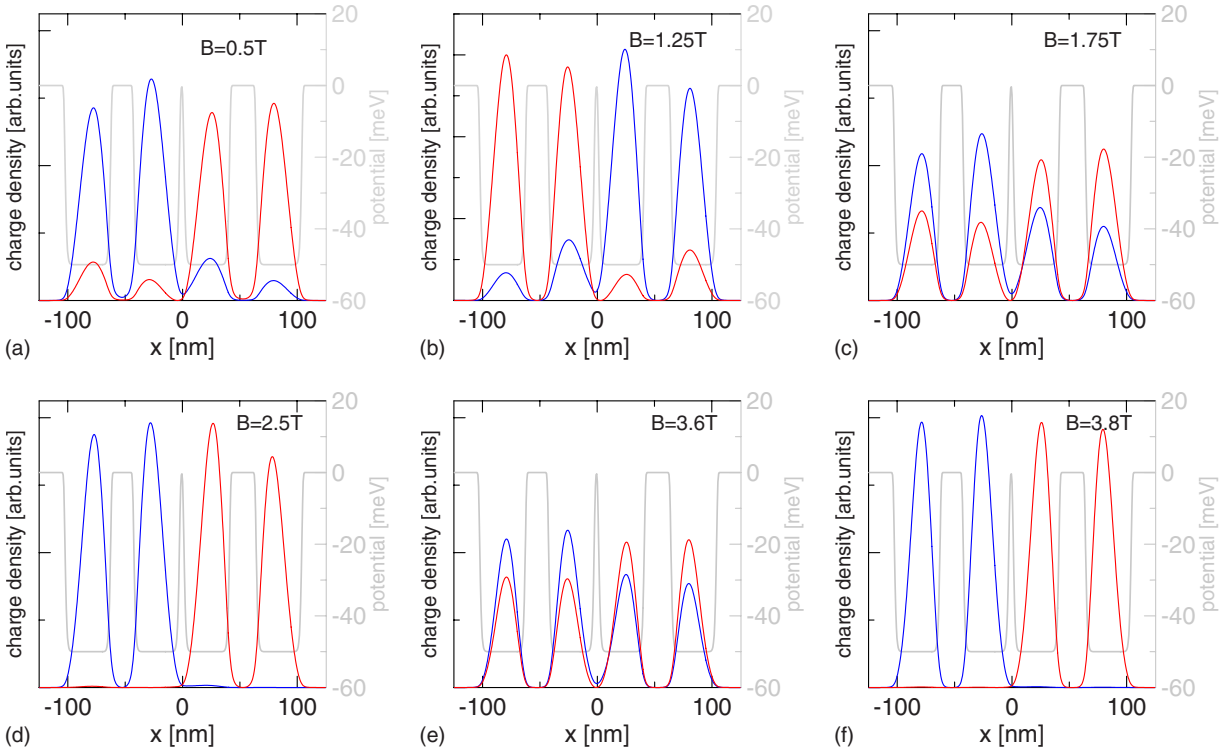

FIG. 25. (Color online) Cross section of the confinement potential (gray lines) and the charge density of the single confined electron in the lowest-energy state [blue (dark gray) curve] and the first-excited state [red (light gray) curve] for a pair of quantum rings with the radius of the right ring larger by 5% and the interring distance parameter $d=3.5$. Panels correspond to different values of the magnetic field given in the figure.

ring become more pronounced as the magnetic field grows, which is related to the reduction in the tunnel coupling with B.

For two electrons the Coulomb repulsion segregates the electrons between the different rings. For $d=3.75$ and $d=3.5$ the charge confined in each of the rings is equal to $1e$ [see Fig. 26(b)]. Only for $d=3.25$ deviations off the equal distribution of the rings occur. We find that these deviations are accompanied by lifting the singlet-triplet degeneracies in the spectrum. The magnetic field leads eventually to the attenuation of the tunnel coupling and segregation of the carriers between the two rings.

In the system of three electrons [see Fig. 26(c)] for large interring barrier ($d=3.75$) two electrons occupy the larger ring, leaving a single electron in the smaller one. For $d=3.5$ the charge accumulated in the smaller ring exceeds one elementary charge for low magnetic fields. For $d=3.25$ the electron distribution between the rings becomes closer to $3e/2$ per ring. Oscillations of the charge in the smaller ring for $d=3.5$ and $d=3.25$ are associated with the avoided crossings that appear in the low-spin part of the spectrum, as well as with the ground-state spin transitions. The latter produce cusps on the plotted curves [see Fig. 26(c)].

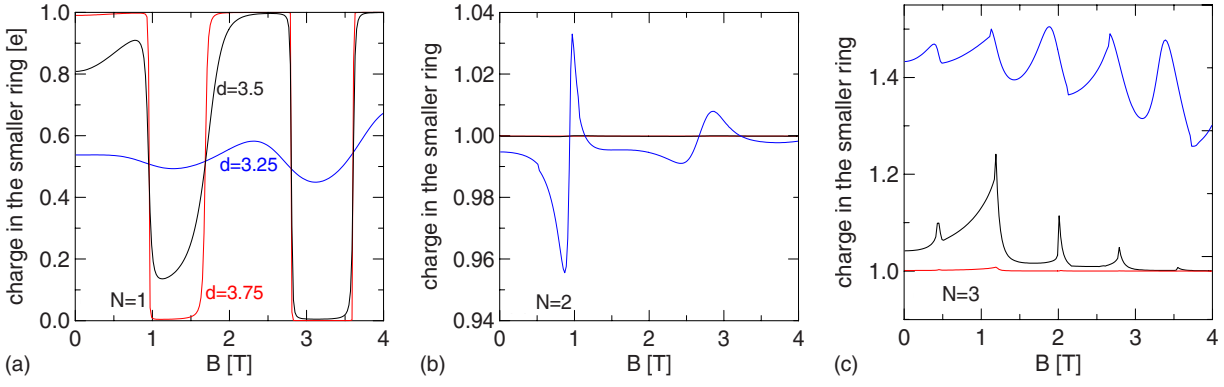

FIG. 26. (Color online) Charge localized in the smaller ring for ground state of the (a) single electron, (b) two electrons, and (c) three electrons for the ring couple with the radius of the right ring larger by 5%. Red (light gray), black, and blue (dark gray) lines correspond to $d=3.75$, $d=3.5$, and $d=3.25$, respectively.

IV. SUMMARY AND CONCLUSIONS

We have studied the system of one, two, and three electrons in a planar double-ring structure considering both the tunnel and the electrostatic coupling between the rings using a Gaussian function mesh technique.

The presented results indicate that in the system of few electrons there is a distinct competition of tunnel coupling with (1) the magnetic field, which enhances localization of the occupied states within a single ring, (2) the electron-electron interaction, which strengthens the interring barrier, and (3) asymmetry effects of the double-ring structure, which favor electron localization in one of the rings.

We find that the system undergoes symmetry transitions of the parity and spin in functions of the magnetic field. At large interring barrier (d) for $N=1$ we find angular momentum transitions for states localized in a single ring. These transitions are absent in the system of two electrons since their mutual interaction perturbs the rotational symmetry of each of the rings. $N=2$ ground state at large d is degenerate with respect to the spin due to the perfect separation of the electrons. For $N=3$ at large d the symmetry transformations are present, and result of the spin transitions within the two-electron subsystem confined in one of the rings. When the rings are identical at large d the ground state is degenerate with respect to the parity for any N.

In the opposite limit of strong interring coupling and coalesced rings we find lifting of the even-odd degeneracy for all the studied electron numbers. The symmetry transformations in functions of the magnetic field vanish for the single electron, which occupies the binding orbital and in the limit of coalesced rings—the quantum dot formed at the contact of the rings. On the contrary, for two electrons the symmetry transformations occur only when the rings form a single structure. For three electrons the symmetry transformations are present at any d. At large d they are only related to the spin transitions of the two-electron subsystem, and in the strong coupling limit they involve both parity and spin. For $d=3$ the sequence of the parity and spin ground-state symmetries in functions of the magnetic field is identical with the one found for strongly deformed elliptic quantum dots.

We demonstrated that due to the strong dependence of the symmetry transformations on both N and d, the confined charge as well as the distance between the rings should be readily accessible in both single-electron charging and magnetization measurements performed in functions of the magnetic field. In particular the strength of the coupling has an opposite impact on the chemical potentials of one and two confined electrons. For weak tunnel coupling μ_1 has cusps in function of the field while μ_2 is a smooth function of B. In the strong-coupling limit the dependence is inverted: chemical potential of the single electron becomes smooth and the cusps appear on μ_2.

The asymmetry in the depth of the confinement potential favors localization of electrons in the deeper potential well. Less obvious is the effect of the asymmetry in the size of the rings. For rings of different radii the magnetic field leads to switching of the ground-state localization from the larger to the smaller rings. The oscillations of the ground-state localization become more abrupt for stronger magnetic fields due to the reduction of the tunnel coupling. Both types of the asymmetry—in the depth and in the size of the ring, for large values of d or B—break the tunnel coupling between the rings by tending to localize the electron in one of the rings—favoring the atomic type of localization over the molecular (extended) one. The asymmetry in the double-ring potential lifts the degeneracy of the even- and odd-parity energy levels that is observed at large d for any N. We find that when d is decreased, the asymmetry effects are reduced. In particular the electron charge between the rings becomes more evenly distributed for the strongly tunnel-coupled asymmetric structures.

ACKNOWLEDGMENTS

This work was partly supported by the Polish Ministry for Science and Higher Education and by the EU Network of Excellence: SANDiE.

APPENDIX

In this appendix we explain how the matrix elements for the Coulomb interaction

$$V_{abcd} = \langle \phi_a(\mathbf{r}_1)\phi_b(\mathbf{r}_2)|\frac{1}{r_{12}}|\phi_c(\mathbf{r}_1)\phi_d(\mathbf{r}_2)\rangle \tag{A1}$$

are integrated. In the above expression the single-electron wave functions are replaced by their linear combinations [Eq. (3)],

$$V_{abcd} = \sum_{i,j,k,l=1}^{N} a_i^* b_j^* c_k d_l \langle f_i(\mathbf{r}_1) f_j(\mathbf{r}_2)|\frac{1}{r_{12}}|f_k(\mathbf{r}_1) f_l(\mathbf{r}_2)\rangle. \tag{A2}$$

An interaction integral which appears in Eq. (A2)

$$C_{ijkl} = \langle f_i(\mathbf{r}_1) f_j(\mathbf{r}_2)|\frac{1}{r_{12}}|f_k(\mathbf{r}_1) f_l(\mathbf{r}_2)\rangle = \int d^2\mathbf{r}_1 \int d^2\mathbf{r}_2 f_i^*(\mathbf{r}_1) f_j^*(\mathbf{r}_2)\frac{1}{r_{12}} f_k(\mathbf{r}_1) f_l(\mathbf{r}_2) \tag{A3}$$

can be calculated in following way. First, we should substitute in place of f_i, f_j, f_k, f_l, and $\frac{1}{r_{12}}$ their inverse Fourier transform. Next step is to integrate over $\mathbf{r}_1$ and $\mathbf{r}_2$ variables. After these we get the formula on C_{ijkl},

$$C_{ijkl} = B_{ijkl}\int d^2\mathbf{k}\frac{1}{k}\exp\left(-\frac{\sigma^2 k^2}{2}\right)\exp(i\mathbf{k}\cdot\mathbf{R})\exp\left(\frac{\gamma\sigma^2}{2}\mathbf{k}\cdot\mathbf{r}\right), \tag{A4}$$

where

$$\mathbf{R} = (X_{ik} - X_{jl}, Y_{ik} - Y_{jl}) = R(\cos\beta, \sin\beta), \tag{A5}$$

$$\mathbf{r} = (y_{jl} - y_{ik}, x_{ik} - x_{jl}) = r(\cos\alpha, \sin\alpha), \tag{A6}$$

$$\mathbf{r}_{ik} = \mathbf{R}_i - \mathbf{R}_k, \tag{A7}$$

$$\mathbf{r}_{jl} = \mathbf{R}_j - \mathbf{R}_l, \tag{A8}$$

$$\mathbf{R}_{ik} = \frac{\mathbf{R}_i + \mathbf{R}_k}{2}, \tag{A9}$$

$$\mathbf{R}_{jl} = \frac{\mathbf{R}_j + \mathbf{R}_l}{2}, \tag{A10}$$

$$\gamma = -\frac{eBa_B^2}{2\hbar}, \tag{A11}$$

a_B is Bohr radius, and

$$B_{ijkl} = \frac{\pi\sigma^4}{2}\exp\left[-\frac{\gamma^2\sigma^2}{4}(\mathbf{r}_{ik}^2 + \mathbf{r}_{jl}^2)\right] \times \exp[i\gamma(-Y_{ik}x_{ik} - Y_{jl}x_{jl} + X_{ik}y_{ik} + X_{jl}y_{jl})] \times \exp\left(-\frac{r_{ik}^2 + r_{jl}^2}{4\sigma^2}\right). \tag{A12}$$

Expression (A4) can be further simplified by transformation of the integral form from Cartesian to cylindrical coordinates and a subsequent integration over the k variable,

$$C_{ijkl} = B_{ijkl}\frac{\sqrt{2\pi}}{2\sigma}\int_0^{2\pi} d\varphi \exp\left(\frac{A^2(\varphi)}{2\sigma^2}\right)\left[1 - \mathrm{erf}\left(\frac{A(\varphi)}{\sqrt{2}\sigma}\right)\right], \tag{A13}$$

where function $A(\varphi)$ is defined as

$$A(\varphi) = -iR\cos(\varphi - \beta) - \frac{\gamma\sigma^2}{2}r\cos(\varphi - \alpha). \tag{A14}$$

Integral (A13) is evaluated numerically.

[1] Y. Aharonov and D. Bohm, Phys. Rev. **115**, 485 (1959).
[2] M. Büttiker, Y. Imry, and M. Y. Azbel, Phys. Rev. A **30**, 1982 (1984).
[3] G. Timp, A. M. Chang, J. E. Cunningham, T. Y. Chang, P. Mankiewich, R. Behringer, and R. E. Howard, Phys. Rev. Lett. **58**, 2814 (1987).
[4] D. Mailly, C. Chapelier, and A. Benoit, Phys. Rev. Lett. **70**, 2020 (1993).
[5] M. Bayer, M. Korkusinski, P. Hawrylak, T. Gutbrod, M. Michel, and A. Forchel, Phys. Rev. Lett. **90**, 186801 (2003).
[6] W. G. van der Wiel, Yu. V. Nazarov, S. De Franceschi, T. Fujisawa, J. M. Elzerman, E. W. G. M. Huizeling, S. Tarucha, and L. P. Kouwenhoven, Phys. Rev. B **67**, 033307 (2003).
[7] A. Lorke, R. J. Luyken, A. O. Govorov, J. P. Kotthaus, J. M. Garcia, and P. M. Petroff, Phys. Rev. Lett. **84**, 2223 (2000).
[8] A. Fuhrer, S. Lüscher, T. Ihn, T. Heinzel, K. Ensslin, W. Wegscheider, and M. Bichler, Nature (London) **413**, 822 (2001).
[9] M. Grochol and R. Zimmermann, Phys. Rev. B **76**, 195326 (2007).
[10] J. I. Climente, J. Planelles, and W. Jaskólski, Phys. Rev. B **68**, 075307 (2003).
[11] A. Puente, L. Serra, and R. G. Nazmitdinov, Phys. Rev. B **69**, 125315 (2004).
[12] N. A. J. M. Kleemans, I. M. A. Bominaar-Silkens, V. M. Fomin, V. N. Gladilin, D. Granados, A. G. Taboada, J. M. Garcia, P. Offermans, U. Zeitler, P. C. M. Christianen, J. C. Maan, J. T. Devreese, and P. M. Koenraad, Phys. Rev. Lett. **99**, 146808 (2007).
[13] S. Viefers, P. Koskinen, P. Singa Deo, and M. Manninen, Physica E (Amsterdam) **21**, 1 (2004).
[14] T. Chakraborty and P. Pietiläinen, Phys. Rev. B **50**, 8460 (1994).
[15] A. O. Govorov, S. E. Ulloa, K. Karrai, and R. J. Warburton, Phys. Rev. B **66**, 081309(R) (2002).
[16] J. I. Climente, J. Planelles, and J. L. Movilla, Phys. Rev. B **70**, 081301(R) (2004).
[17] Y. V. Pershin and C. Piermarocchi, Phys. Rev. B **72**, 125348 (2005).
[18] V. M. Fomin, V. N. Gladilin, S. N. Klimin, J. T. Devreese, N. A. J. M. Kleemans, and P. M. Koenraad, Phys. Rev. B **76**, 235320 (2007).
[19] V. M. Fomin, V. N. Gladilin, J. T. Devreese, N. A. J. M. Kleemans, and P. M. Koenraad, Phys. Rev. B **77**, 205326 (2008).
[20] P. Földi, O. Kálmán, M. G. Benedict, and F. M. Peeters, Nano Lett. **8**, 2556 (2008); O. Kálmán, P. Földi, M. G. Benedict, and F. M. Peeters, Phys. Rev. B **78**, 125306 (2008).
[21] B. Szafran, Phys. Rev. B **77**, 205313 (2008).
[22] T. Kuroda, T. Mano, T. Ochiai, S. Sanguinetti, K. Sakoda, G. Kido, and N. Koguchi, Phys. Rev. B **72**, 205301 (2005).
[23] T. Mano, T. Kuroda, S. Sanguinetti, T. Ochiai, T. Tateno, J. Kim, T. Noda, M. Kawabe, K. Sakoda, G. Kido, and N. Koguchi, Nano Lett. **5**, 425 (2005).
[24] A. Mühle, W. Wegscheider, and R. J. Haug, Appl. Phys. Lett. **91**, 133116 (2007).
[25] D. Granados, J. M. García, T. Ben, and S. I. Molina, Appl. Phys. Lett. **86**, 071918 (2005); F. Suárez, D. Granados, M. L. Dotor, and J. M. García, Nanotechnology **15**, S126 (2004).
[26] B. Szafran and F. M. Peeters, Phys. Rev. B **72**, 155316 (2005).
[27] J. Planelles and J. I. Climente, Eur. Phys. J. B **48**, 65 (2005).
[28] J. I. Climente, J. Planelles, M. Barranco, F. Malet, and M. Pi, Phys. Rev. B **73**, 235327 (2006).
[29] F. Malet, M. Pi, M. Barranco, E. Lipparini, and L. Serra, Phys. Rev. B **74**, 193309 (2006).
[30] L. K. Castelano, G.-Q. Hai, B. Partoens, and F. M. Peeters, Phys. Rev. B **74**, 045313 (2006).
[31] B. Szafran, S. Bednarek, and M. Dudziak, Phys. Rev. B **75**, 235323 (2007).
[32] G. Piacente and G. Q. Hai, J. Appl. Phys. **101**, 124308 (2007).
[33] L. G. G. V. Dias da Silva, J. M. Villas-Bôas, and S. E. Ulloa, Phys. Rev. B **76**, 155306 (2007).
[34] J. I. Climente and J. Planelles, J. Phys.: Condens. Matter **20**,

035212 (2008).
[35] A. Harju, S. Siljamäki, and R. M. Nieminen, Phys. Rev. Lett. **88**, 226804 (2002).
[36] S. M. Reimann and M. Manninen, Rev. Mod. Phys. **74**, 1283 (2002).
[37] P.-O. Lowdin, Rev. Mod. Phys. **36**, 966 (1964).
[38] G. Burkard, D. Loss, and D. P. DiVincenzo, Phys. Rev. B **59**, 2070 (1999); D. Bellucci, M. Rontani, F. Troiani, G. Goldoni, and E. Molinari, *ibid.* **69**, 201308(R) (2004); S. Bednarek, T. Chwiej, J. Adamowski, and B. Szafran, *ibid.* **67**, 205316 (2003); X. Hu and S. Das Sarma, Phys. Rev. A **61**, 062301 (2000); L.-X. Zhang, D. V. Melnikov, S. Agarwal, and J.-P. Leburton, Phys. Rev. B **78**, 035418 (2008).
[39] W. Häusler and B. Kramer, Phys. Rev. B **47**, 16353 (1993); B. Szafran, F. M. Peeters, S. Bednarek, T. Chwiej, and J. Adamowski, *ibid.* **70**, 035401 (2004); T. Sako and G. H. F. Diercksen, J. Phys.: Condens. Matter **20**, 155202 (2008).
[40] $(1+P_{12})$ in Eq. (9) ensures the symmetry of the wave function with respect to the electron exchange and simultaneously even spatial parity of the state. For $d>3.5$ in the ground state the even singlet is degenerate with the odd triplet. The odd triplet is obtained for $(1+P_{12})$ replaced by $(1-P_{12})$. As long as the electron tunneling between the rings is negligible (as long as the radial functions χ_l and χ_r are separated) the two-electron density is the same for both the states.
[41] K. Niemelä, P. Pietiläinen, P. Hyvönen, and T. Chakraborty, Europhys. Lett. **36**, 533 (1996).
[42] S. A. Mikhailov and N. A. Savostianova, Phys. Rev. B **66**, 033307 (2002).
[43] B. Szafran, F. M. Peeters, S. Bednarek, and J. Adamowski, Phys. Rev. B **69**, 125344 (2004).
[44] Y. Li, C. Yannouleas, and U. Landman, Phys. Rev. B **76**, 245310 (2007).